

Geophysical Research Letters

RESEARCH LETTER

10.1029/2018GL080025

Key Points:

- Seismic model EARA2014 beneath Japan shows intermediate-depth and deep earthquakes occur in the top 60 km of the subducted Pacific Plate
- The lower plane of the double seismic zones at 100- to 380-km depths corresponds to a slab mantle with temperatures between 400 and 900 degrees Celsius
- Dehydration of hydrous minerals in the slab mantle may facilitate deep earthquake genesis through the released water

Supporting Information:

- Supporting Information S1
- Data Set S1

Correspondence to:

M. Chen,
chenmi22@msu.edu

Citation:

Chen, M., Manea, V. C., Niu, F., Wei, S. S., & Kiser, E. (2019). Genesis of intermediate-depth and deep intraslab earthquakes beneath Japan constrained by seismic tomography, seismicity, and thermal modeling. *Geophysical Research Letters*, 46, 2025–2036. <https://doi.org/10.1029/2018GL080025>

Received 12 AUG 2018

Accepted 31 JAN 2019

Accepted article online 6 FEB 2019

Published online 21 FEB 2019

Genesis of Intermediate-Depth and Deep Intraslab Earthquakes beneath Japan Constrained by Seismic Tomography, Seismicity, and Thermal Modeling

Min Chen^{1,2} , Vlad Constantin Manea^{3,4}, Fenglin Niu^{5,6} , S. Shawn Wei², and Eric Kiser⁷ 

¹Department of Computational Mathematics, Science and Engineering, Michigan State University, East Lansing, MI, USA, ²Department of Earth and Environmental Sciences, Michigan State University, East Lansing, MI, USA,

³Computational Geodynamics Laboratory, Centro de Geociencias, Universidad Nacional Autónoma de México, Campus Juriquilla, Querétaro, Mexico, ⁴Astronomical Institute of the Romanian Academy, Bucharest, Romania, ⁵Department of Earth Science, Rice University, Houston, TX, USA, ⁶State Key Laboratory of Petroleum Resource and Prospecting, and Unconventional Natural Gas Institute, China University of Petroleum, Beijing, China, ⁷Department of Geosciences, University of Arizona, Tucson, AZ, USA

Abstract The distribution of intermediate-depth and deep intraslab earthquakes with respect to subducting slabs offers a unique insight into seismogenesis at high pressures and temperatures that should inhibit brittle failure. This study constrains the surface of the subducting Pacific Plate beneath Japan at depths between 100 and 380 km based on a previous continental-scale adjoint tomography model. Earthquake distributions relative to the slab surface reveal double seismic zones located within the top 60 km of the Pacific Plate. Thermal modeling suggests that the lower-plane seismicity corresponds to temperatures between 400 and 900 °C. The seismogenic pressure and temperature conditions correlate approximately with the conditions of dehydration reactions of several hydrous minerals, that is, antigorite (serpentine) and chlorite at depths between 100 and 200 km and phase A at greater depths between 200 and 380 km. These correlations indicate that at these depths water released from dehydration processes may facilitate triggering slab mantle earthquakes.

Plain Language Summary Most earthquakes below 70 km are thought to occur within subducting oceanic plates. The cause of these intermediate-depth and deep earthquakes is still enigmatic because at high pressure-temperature environments brittle fractures are not expected to happen. Various earthquake mechanisms have been proposed, but differentiating them is challenging, partly due to the resolution limitations in seismic imaging of both the subducting plate structure and the earthquake sources. This study defines the deep interface of the subducting Pacific Plate beneath Japan using an improved model, obtained with an advanced seismic imaging technique. We discover vertically varying double seismic zones located within the top 60 km of the plate at 100- to 380-km depths. The calculated pressure-temperature conditions of the lower plane of the double seismic zone are correlated with the conditions at which a series of hydrous minerals break down into water and solids. This correlation suggests that water released from breakdown of hydrous minerals likely raises pore-fluid pressure and triggers intermediate-depth and deep earthquakes similar to the process of hydraulic fracturing.

1. Introduction

Intermediate-depth (70- to 300-km deep) and deep (300- to 700-km deep) intraslab earthquakes are poorly understood because at these depths the high pressure-temperature (P - T) conditions should inhibit brittle failure. Various mechanisms have been proposed to explain the triggering of these earthquakes, which include geometric unbending of the elastic core of the slab (Engdahl & Scholz, 1977; Kao & Ruey-Juin, 1999; Kawakatsu, 1985; McGuire & Wiens, 1995), thermal shear instability due to a positive feedback between deformation-induced heating and deformation (Hobbs & Ord, 1988; John et al., 2009; Karato et al., 2001; Ohuchi et al., 2017), dehydration embrittlement caused by breakdown of hydrous minerals and subsequently in situ positive volume change (Dobson et al., 2002; Jung et al., 2004; Kirby et al., 1996; Okazaki & Hirth, 2016; Peacock, 2001; Yamasaki & Seno, 2003), fluid-related embrittlement related to the presence of fluid in general (Van Keken et al., 2012; Wei et al., 2017), and phase transformational faulting

along the boundaries of metastable mineral wedges (Green & Houston, 1995; Kao & Liu, 1995; Kirby et al., 1991). Identifying the viable mechanisms requires accurate modeling of temperature, pressure, stress, rheology, and composition of the intraslab seismogenic zones, which ultimately depends on robust seismic constraints of slab structural details and earthquake locations.

The intraslab seismogenic zone beneath northeast Japan is particularly well studied due to its high seismicity rate and dense seismic station coverage within Japan. A double seismic zone (DSZ) is observed with two planes of seismicity 40 km apart at 50-km depth and merging into one single seismic plane at around 200-km depth (Hasegawa et al., 1978, 1994). High-resolution seismic images suggest that the upper seismic plane is located mostly within the slab oceanic crust, whereas the lower plane is situated within the slab mantle (Igarashi et al., 2001; Shiina et al., 2013; Zhang et al., 2004). Dehydration embrittlement or more generally fluid-related embrittlement is invoked to explain the vertical extent and relative locations of the DSZ with respect to the slab top, owing to the spatial correspondence between the two seismic planes and the modeled dehydration loci of slab metamorphic facies (Hacker et al., 2003; Van Keken et al., 2012; Yamasaki & Seno, 2003). In the fluid-related embrittlement process, water released from in situ dehydration reactions or transported from elsewhere increases pore-fluid pressure, reduces effective normal stress, and therefore helps trigger earthquakes (Faccenda et al., 2012; Van Keken et al., 2012; Wei et al., 2017). However, questions remain regarding if the mechanism of fluid-related embrittlement keeps operating to promote intraslab earthquakes at greater depths and pressure (>200 km, or ~6 GPa), where the slab is relatively less well constrained due to insufficient seismicity and a lack of seismic data coverage. The slab top surface below 150 km has been generally fit by a deep seismicity contour (e.g., Hayes et al., 2012; Syracuse & Abers, 2006), which may not capture the true slab surface geometry. This can hinder meaningful thermal modeling of deep seismogenic zones and limit our ability to understand the thermal and petrological environments that promote deep intraslab earthquakes.

Instead of approximating the top of the slab based upon deep seismicity, this study employs an alternative approach by defining the slab surface beneath Japan based upon a recent continental-scale tomographic model EARA2014 (Chen et al., 2015). This new slab surface location is then used to establish bimodal Gaussian distributions of seismicity in the subducting Pacific Plate, assuming double-planed seismic zones at depths between 100 and 380 km (Figure 1). We further estimate the slab thermal structure to examine petrological implications of the relative positions of lower-plane seismic zones within the slab at different depth ranges.

2. Methods and Data

2.1. Adjoint Tomography and Model Comparison

Aided by both dense wide-aperture seismic networks in East Asia (mainly in China and Japan) and adjoint tomography (Tromp et al., 2005), an advanced full waveform tomography technique, an East Asia Radially Anisotropic Model (EARA2014) including the Japan subduction zone was obtained with an improved resolution from global-scale tomographic models (Chen et al., 2015; supporting information Text S1). Adjoint tomography takes into account full 3-D wave propagation effects and off-raypath sensitivity (Tromp et al., 2005). Therefore, it is theoretically more accurate than the traditional ray theory-based tomography (e.g., Liu & Tromp, 2008; Tape et al., 2009; Zhu et al., 2012). Seismic structures in EARA2014 is especially better resolved at depths below 150 km with the help of dense and wide-aperture station coverage in China, compared to the previous high-resolution traveltime tomographic models (e.g., Shiina et al., 2013; Zhang et al., 2004), for the reason that the previous traveltime tomographic methods particularly rely on abundant subduction related seismicity at shallower depths, which diminishes at greater depths. However, at depths shallower than 150 km, the resolution of model EARA2014 suffers from sparse local data coverage due to the very limited number of shallow earthquakes used as well as the irregular station coverage; that is, stations are lacking in the back arc and the trench outer rise regions but only are concentrated on Japan islands. Further details on the model resolution may be found in supporting information Text S2.

The dataset used in the adjoint tomography consists of 1.7 million frequency-dependent traveltime measurements, from a total of 227 earthquakes in East Asia, 32 of which are within the Japan region and only 10 of which are below 100 km. Therefore, model EARA2014 at depths larger than 150 km captures the 3-D Pacific Plate wave speed structure without a priori information of a large number of deep earthquakes, but instead

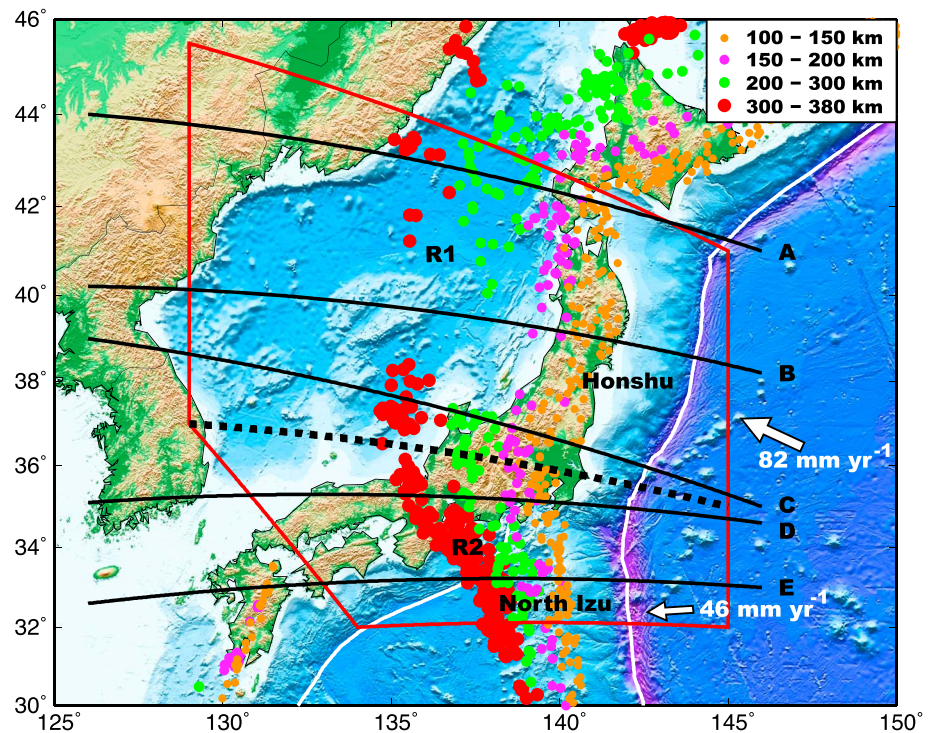


Figure 1. Map of the EHB epicenter distribution in Japan. The EHB earthquake hypocenter data are from years 1960 to 2008. Colored circles mark the epicenters in different depth ranges indicated by the map legend (top right corner). Black solid lines indicate five profiles marked by A–E, along which cross sections of seismic wave speed anomalies are shown in Figures 2, S7a, S7b, and S10. The red box encloses all the epicenters analyzed in this study. The boxed region is further divided by the thick black dashed line into regions R1 associated with the Honshu arc and R2 with the North-Izu arc. The white arrows indicate the Pacific Plate arc-normal convergence directions and rates in a Eurasia reference frame. The white lines delineate the trench axis.

using multiple seismic phases recorded by a large number of stations. The model construction and validation have been discussed in a previous publication (Chen et al., 2015). Here we focus on analyzing the high-wave speed (high- V) anomalies in the model that represent the subducting Pacific Plate beneath the Honshu and the North-Izu regions (Figure 1) and the position of intraslab seismicity relative to the interpreted slab top surface.

Similar to the other continental-scale tomographic models (e.g., Liu & Zhao, 2016; Wei et al., 2012), model EARA2014 (Figures 2a and 2b) does not reveal the detailed internal structures of the slab. Low-wave speed waveguides associated with a metamorphosed oceanic crust (Abers, 2005; Bock et al., 2000; Kawakatsu & Yoshioka, 2011; Nakajima et al., 2009; Shiina et al., 2013) and possibly a serpentinized slab mantle (Chen et al., 2007; Nakajima et al., 2009; Zhang et al., 2004) are not resolvable since only low-frequency body waves with minimum periods of 12 s are used in the adjoint tomography. Without a clear indication of oceanic crust, we employ a proxy of the slab surface using the 2% contour of shear wave speed anomalies ($\delta \ln V_S$) from EARA2014 (Figures 2a and 2b). This approximation places a majority of the earthquakes below and in the vicinity of the slab top surface (supporting information Text S3).

Compared to the global-scale tomographic models such as GAP_P4 (Fukao & Obayashi, 2013; Obayashi et al., 2013; Figures S7a and S7b) and SL2013Vs (Schaeffer & Lebedev, 2013; Figure S10a), the interpreted slab top from EARA2014 aligns more closely with deep seismicity (Figures 2a and 2b). Beneath south Japan along profile D, EARA2014 reveals a well-established high- V slab (i.e., the subducting Pacific Plate) with $\delta \ln V_S$ more than 2% at depths between 300 and 400 km next to a cluster of deep earthquakes (Figure 2b), while in the same region GAP_P4 exhibits a possible slab gap with weakly high- V P wave anomalies ($\delta \ln V_P$) of less than 0.5% (Figure S7b) and SL2013Vs starts to lose resolution of the slab at a depth of 300 km (Figure S10a). The close alignment of deep seismicity and the slab top is also shown in other high-

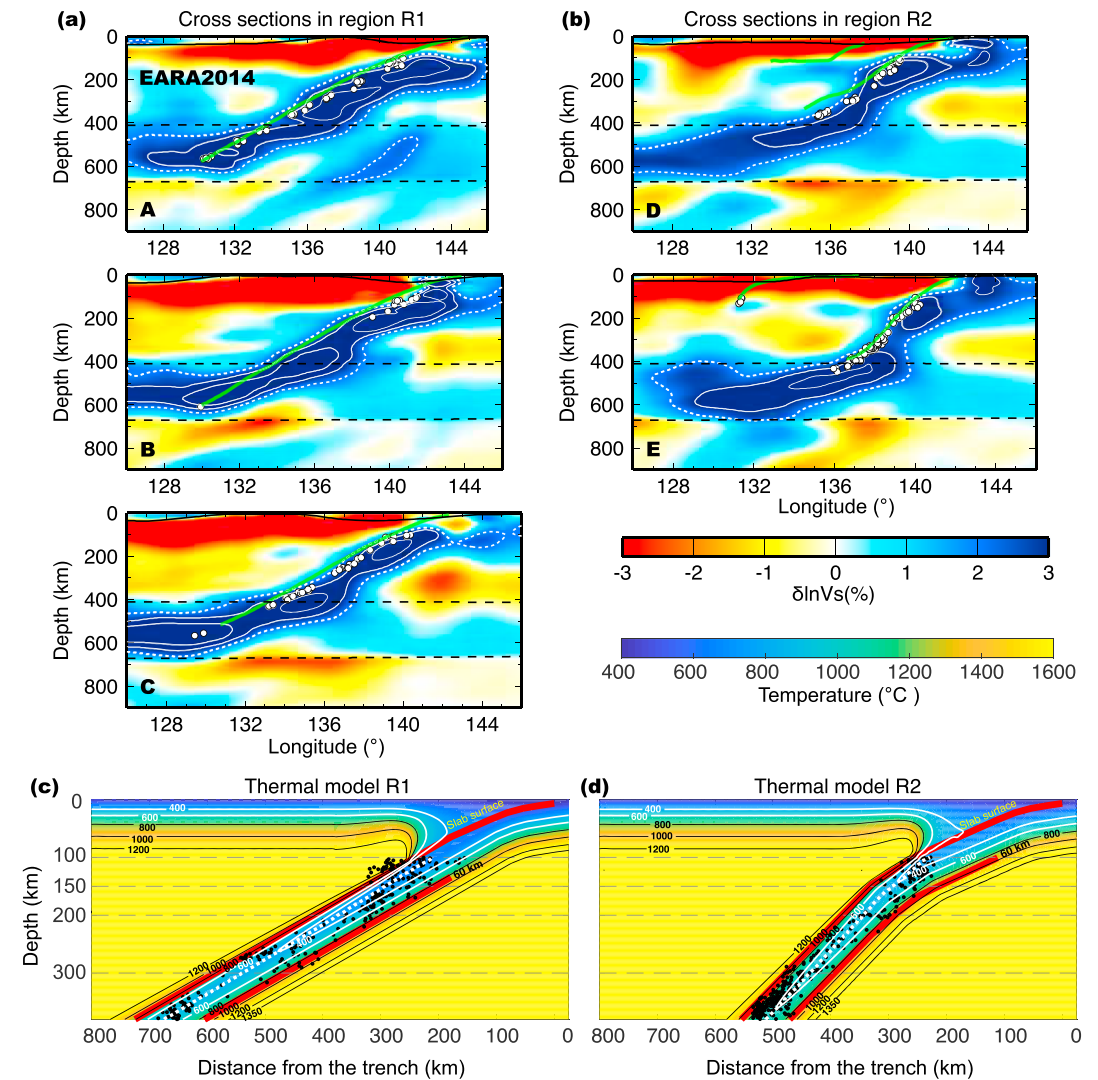


Figure 2. Slab model from EARA2014 and slab thermal models. (a) Cross sections of shear wave speed anomalies $\delta \ln V_S$ along profiles A–C in region R1 (Figure 1). (b) Cross sections along profiles D and E in region R2 (Figure 1). In a and b the earthquakes (white circles) are within 25-km distance of each cross section, white dashed lines mark a $\delta \ln V_S$ contour level of 2% as the interpreted Pacific Plate and white solid lines represent contour levels of 3% and 4%. Black dashed lines mark the 410 and 660 discontinuities, and green lines delineate the slab top surface from model Slab1.0. (c) Slab thermal modeling for region R1 using a flat slab with a constant dip angle of 24° below 100 km. (d) Slab thermal modeling for region R2 using a steep slab with a dip angle of 33° at depths between 100 and 150 km and a dip angle of 46° at depths greater than 150 km. In (c) and (d) black circles denote deep earthquake locations with slab-normal depths calculated from the EARA2014 slab top. The temperature contours are plotted at 200 °C interval in thin white lines (400 °C and 600 °C) or black lines (800–1200 °C). The slab bottom interface is defined by a temperature contour of 1350 °C (the mantle potential temperature), indicated by the thick black line. White dashed lines indicate the coldest slab thermal center at depths greater than 100 km. Gray dashed lines mark the depths at 100, 150, 200, and 300 km.

resolution regional tomography models Wei2012_Vp (Wei et al., 2012; Figure S10b) and Liu2016_Vs (X. Liu & Zhao, 2016, their Figure 15). However, in both regional models, Wei2012_Vp (cross sections along profiles D and E in Figure S10b) and Liu2016_Vs (their Figure 18 in Liu & Zhao, 2016), apparent slab gaps also exist beneath south Japan, likely due to differences in data coverage and tomography techniques, versus actual gaps in the slab.

The slab top interface in general is better resolved than the slab bottom interface, because it is a sharper seismic discontinuity and more seismic waves are available to sample the upper boundary of the slab. On the other hand, below ~100 km and above the mantle transition zone, the position of the slab bottom

boundary can be drastically different even though the subduction top interface is consistently determined by continental-scale tomographic studies (e.g., EARA2014, Wei2012_Vp, and Liu2016_Vs). In the study of Liu and Zhao (2016) the local *S* wave traveltimes tomography produces a skinny slab of about 50-km thick, while the joint tomography of local, teleseismic body and surface waves yields a more robustly constrained slab with a thickness of about 100 km, more consistent with the receiver-function study result beneath Japan, that is, a thickness of ~90 km for a 130-Myr-old oceanic lithosphere (Kumar & Kawakatsu, 2011). In model EARA2014 the imaged slab (~150-km thick) appears to be thicker due to the low-frequency body waves used. Imaging the slab bottom boundary can be improved in future full waveform inversions by including higher-frequency waves that have shorter wave lengths and better resolve the slab bottom boundary (e.g., teleseismic converted waves).

2.2. Slab-Normal Seismicity Distribution and Thermal Modeling

In order to characterize the spatial relationships between the deep seismogenic zone and the imaged subducting Pacific Plate, we use earthquake hypocenter locations from the EHB catalog (Engdahl et al., 1998), which contains 601 deep earthquakes in our study region at depths between 100 and 380 km from years 1960 to 2008 with body wave magnitudes (*M_b*) of 3–7 (Figure 1). Deep earthquake hypocenters are better determined by the teleseismic solutions of EHB, which are less affected by the slab than the regional solutions of Japan Meteorological Agency (Engdahl et al., 1982; Kisslinger, 1993; Utsu, 1975). We define the earthquake slab-normal depth as the shortest distance between the earthquake hypocenter and the slab top surface, with a positive sign for hypocenters located below and a negative sign for those located above. Histograms of the earthquake slab-normal depths derived from EARA2014 slab surface model are plotted with a bin size of 5 km (Figure 3). We fit the histograms with bimodal Gaussian distributions to characterize the potential double seismic planes at different depth ranges.

To quantify the temperatures of deep earthquake loci, we develop two 2-D slab thermal models (Figures 2c and 2d) based on the distinct slab geometries observed in model EARA2014 beneath regions R1 and R2, respectively (Figures 2a and 2b); that is, the subducting Pacific Plate gets steeper from the north to the south. Therefore, thermal model R1 for the Honshu segment of the Pacific Plate is set up with a constant slab dip angle of 24° below 100 km (Figure 2c) and thermal model R2 for the North Izu segment with steep dip angles (33° between 100 and 150 km and 46° below 150 km; Figure 2d). The details of the thermal modeling method are described in supporting information Text S5. Thermal model R1 associated with Honshu arc assumes a 85-km thick slab (Kumar & Kawakatsu, 2011), a plate age of 130 Myr (Müller et al., 2008), and an arc-normal plate convergence rate of 82 mm/year (DeMets et al., 2010). The North-Izu segment of the Pacific Plate (Figure 1) is slightly older (~135 Myr); thus, thermal model R2 incorporates a slightly thicker slab (90-km thick) with an arc-normal plate convergence rate of 46 mm/year (Syracuse & Abers, 2006). With a similar slab thickness for both thermal models, the slab temperature variations are mainly controlled by the combination of the slab dip angle and the arc-normal plate convergence rate (Figures 2c and 2d).

More detailed discussions on the adjoint tomography of model EARA2014, the model resolution tests, the slab surface modeling assumptions, the uncertainties in earthquake locations, and the slab thermal modeling can be found in the supporting information (Bassin et al., 2000; Chen et al., 2015; Ekström et al., 2005; Fichtner & Trampert, 2011; Gudmundsson & Sambridge, 1998; Hjörleifsdóttir & Ekström, 2010; Komatitsch & Tromp, 2002a, 2002b; Kustowski et al., 2008; Liu et al., 2004; Liu & Tromp, 2006, 2008; Maggi et al., 2009; Manea et al., 2004; Meng et al., 2014; National Geophysical Data Center, 2006; Smith & Ekström, 1997; Stein & Stein, 1992; Syracuse & Abers, 2006; Syracuse et al., 2010; Tape et al., 2010; Tromp et al., 2005; Zhan et al., 2014; Zheng et al., 2009; Zhu et al., 2012).

3. Results

In both thermal models (R1 and R2) the coldest temperature within the slab (T_{\min}) increases with depth. In thermal model R1, T_{\min} increases from about 210 °C at 100 km depth to about 560 °C at 380-km depth. Compared to thermal model R1, the combined effect of a steeper slab and a slower arc-normal plate convergence rate in thermal model R2 leads to a slightly warmer slab (about 40 °C warmer of T_{\min}) at a shallow depth of 100 km, and a similar T_{\min} at greater depths (Figures 2c, 2d, 3, 4a, and 4b). On the other hand, the coldest slab core in model R1 is located about 10 km away from the slab top at shallow depths

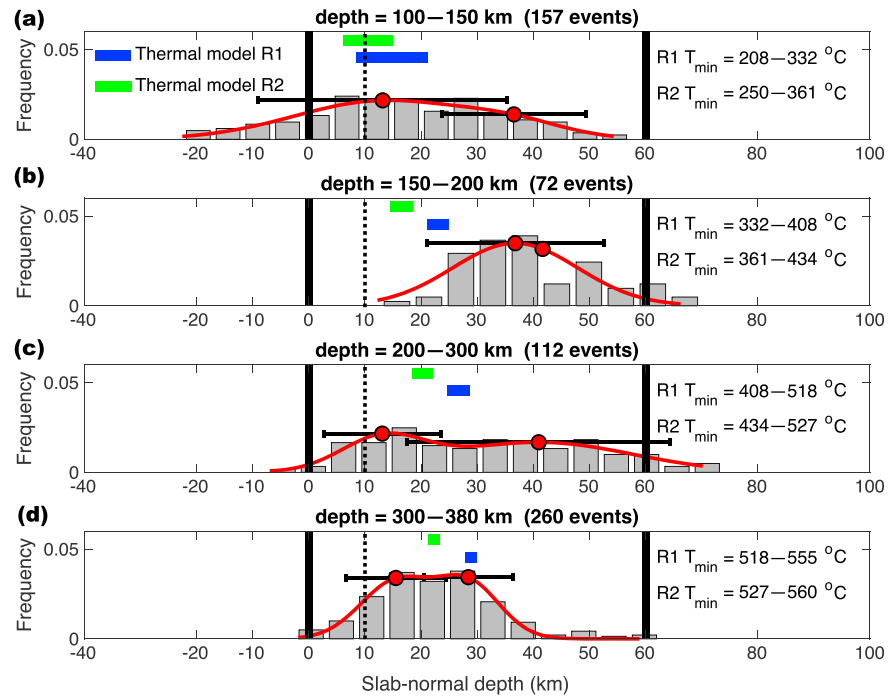


Figure 3. Histograms of the slab-normal depths of deep seismicity calculated based on a slab top surface interpreted from model EARA2014 with 2% contour surface of shear wave speed anomalies. Deep seismicity frequency is plotted as a function of slab-normal depths with a 5 km bin in different depth ranges: (a) 100–150 km, (b) 150–200 km, (c) 200–300 km, and (d) 300–380 km. The thick black lines mark the slab top surface (0 km) and 60 km below the slab top surface. Black dashed lines indicate the slab Moho position. Histograms are modeled with bimodal Gaussian distributions (red lines) with means (red circles) and standard deviations (black error bars). Green and blue horizontal bars indicate the coldest slab region derived from slab thermal models R1 and R2. The values of the coldest temperature in each depth range are indicated by the numbers following T_{min} .

(100–150 km) and up to 25 km at greater depths (300–380 km), while the coldest core of model R2 deepens slightly more into the slab (~2- to 7-km deeper; Figure 3).

Histograms of earthquake slab-normal depths derived from model EARA2014 exhibit bimodal Gaussian distributions that vary with depths (Figure 3). In the depth range of 100–150 km, the bimodal Gaussian model reveals a wide seismogenic zone with two broad seismicity peaks about 25 km apart (Figure 3a), consistent with the widely observed Japan DSZ (Abers et al., 2013; Yamasaki & Seno, 2003). Our results indicate that the upper-plane seismicity peak is located about 12 km below the slab top, presumably close to the slab crust determined by Tsuji et al. (2008), while the lower-plane seismicity peak is situated between 25 and 55 km below the slab top, that is, in the slab mantle. At depths of 150–200 km, the seismicity disappears completely in the top 25 km of the slab, the seismogenic zone width reduces, and two peaks of seismicity merges around a slab-normal depth of 30–40 km (Figure 3b). At depths of 200–300 km, the seismogenic zone widens with two seismicity peaks about 30 km apart (Figure 3c). The upper-plane seismicity peak emerges near the slab Moho, and the lower-plane seismicity peak is located 30–50 km into the slab. At depths of 300–380 km the seismogenic zone tapers again toward the slab coldest core, which is about 22 (in thermal model R1) and 29 km (in thermal model R2) below the slab top (Figure 3d).

4. Discussion

Comparison between the slab thermal models and the deep earthquake loci shows that the majority of the earthquakes (92%) occur in the top 60 km of the EARA2014 slab (Figures 2c, 2d, and 3), corresponding to temperatures below 1000 °C, consistent with the previous studies (Hacker et al., 2003; Peacock, 2001). Due to location uncertainties, the intermediate-depth earthquake distribution from EHB catalog tends to be more scattered compared to the refined hypocenter locations (Kita et al., 2010), which concentrate in

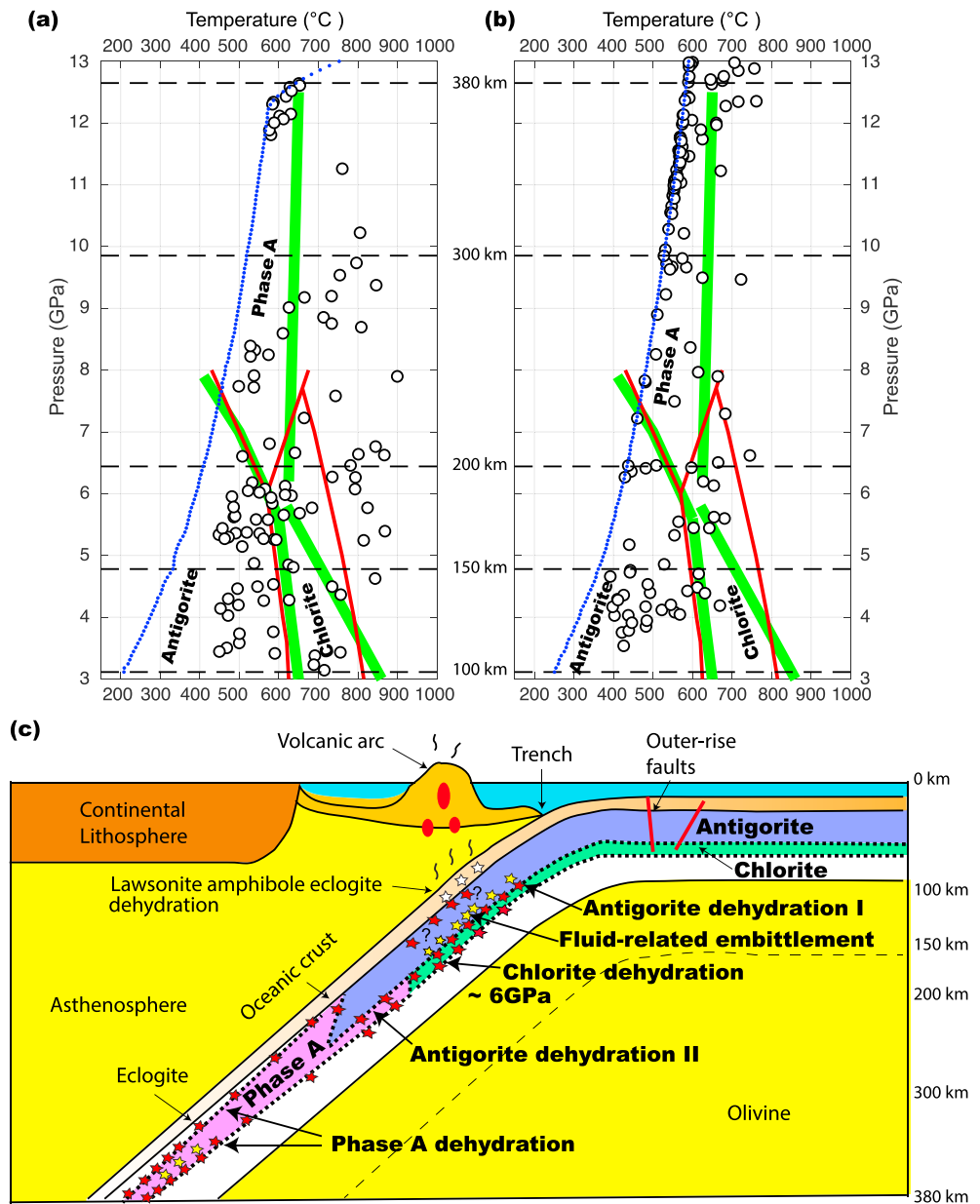


Figure 4. Relationship between dehydration reactions and deep earthquakes within the slab. (a) *P-T* conditions of the earthquakes in the lower-plane seismic zone of Honshu (region R1), denoted by open circles, modeled with slab thermal model R1. (b) *P-T* conditions of the earthquakes in the lower-plane seismic zone of North Izu (region R2), denoted by open circles, modeled with slab thermal model R2. In (a) and (b) the blue dotted lines indicate the *P-T* trajectory of the coldest slab thermal center. Red lines are the hydrous phase boundaries from Hacker et al. (2003), and green thick lines are the dehydration-reaction curves from Omori et al. (2004). (c) Cartoon of slab seismogenesis beneath Japan. Earthquakes occurring in the slab crust are denoted by white stars and in the slab mantle are red and yellow stars. The intraslab deep earthquakes are associated with water released in situ due to different stages of dehydration processes (red stars) or transported from elsewhere (yellow stars): (1) 100–150 km: dehydration reactions of lawsonite amphibole eclogite in the slab crust, antigorite = forsterite + enstatite + H₂O (antigorite dehydration I) and chlorite + enstatite = forsterite + pyrope + H₂O in the slab mantle lithosphere, (2) 150–200 km: reactions of antigorite dehydration I and chlorite dehydration in the slab mantle lithosphere, (3) 200–300 km: reactions of antigorite = phase + enstatite + H₂O (antigorite dehydration I) and phase A + enstatite + Mg-sursassite = pyrope + H₂O in the slab mantle lithosphere, and (4) 300–380 km: dehydration reaction of phase A in the slab mantle lithosphere. Note that the phase A reaction is nearly isothermal according to Omori et al. (2004). Phase boundaries indicated by thick dashed lines. Thin gray dashed lines indicate the slab bottom imaged in tomographic model EARA2014, which is much thicker than the 90-km thick slab thermal model.

the top 40 km of the slab, with a slab-mantle seismicity peak about 30 km away from a slab surface approximated by the upper-plane seismicity envelope. This implies that it is possible that in reality, the slab-mantle earthquakes occur in a slightly colder temperature region. The thermal contours of the slab are highly asymmetric (Figures 2c and 2d). The region close to the slab top surface has much larger thermal gradients and small uncertainties in the locations of earthquakes can lead to large changes in the estimated temperatures of earthquake loci. Therefore, we will focus on discussing only the lower-plane seismic zone at slab-normal depths of 25–55 km, which corresponds to temperatures between 400 and 900 °C at depths of 100–380 km (Figures 3 and 4a and 4b). The errors in the calculated temperatures of the lower-plane seismic zone are estimated to be around 100 °C, if we assume an error of 10 km in the slab-normal position of the earthquakes. Additionally, the slab thermal models of this study are similar to the D80 models beneath Honshu and Izu by Syracuse et al. (2010) with small temperature differences, for example, up to 60 °C beneath Honshu and up to 20 °C beneath Izu at 240-km depth, due to different input parameters used, such as the slab dip angle and the plate convergence rate.

The two seismicity peaks at depths of 100–150 km are less sharp (Figure 3a) than the ones from the previous studies (Hasegawa et al., 1994; Kita et al., 2010), which used a large number of precisely relocated earthquakes for a narrow arc segment. The subdued seismicity peaks can be caused by the uncertainties associated with locations of EHB catalog earthquakes and the interpreted slab top surface along the entire Honshu and North-Izu arc. However, the depth variations of bimodal Gaussian distributions of seismicity, indicating two seismic planes being 25 km apart at the shallower depths (Figure 3a) and merging into one plane at greater depths (Figure 3b), are consistent with previously observed geometries of Benioff DSZ in this region (Abers et al., 2013; Brudzinski et al., 2007; Hasegawa et al., 1994; Kita et al., 2010; Yamasaki & Seno, 2003). It is notable that the slab surface beneath region R1 (Figure 1) is less well resolved at the shallower depth range (100–150 km; Figure 2c) with a small percentage of the earthquakes (~7%) located above the slab. This can bias the absolute slab-normal positions of the seismicity peaks toward the slab surface. However, the relative separation of two seismic layers should not be affected significantly.

It is commonly accepted that the upper seismic plane of the DSZ beneath northeast Japan is associated with dehydration of metamorphosed basalt in the slab crust (e.g., blueschist, lawsonite, and amphibole; Kita et al., 2006; Van Keken et al., 2012), while the lower seismic plane is linked to dehydration of metamorphosed peridotite in the slab mantle (e.g., antigorite serpentine; Brudzinski et al., 2007; Hacker et al., 2003; Hasegawa & Nakajima, 2017; Peacock, 2001). At the Japan trench the fault network of new and ancient faults facilitates the water penetration and hydration of the oceanic lithosphere including the slab mantle (Fujie et al., 2018; Kita & Ferrand, 2018). The hydrous minerals (e.g., antigorite serpentine) in the deep slab mantle require plate hydration prior to its subduction. Different mechanisms of plate hydration have been speculated: (1) normal faulting in the trench outer rise region may provide the seawater pathway to hydrate the oceanic mantle lithosphere to a depth of 30–40 km (Contreras-Reyes et al., 2011; Peacock, 2001; Ranero et al., 2003; Shillington et al., 2015; van Avendonk et al., 2011) and (2) water can be injected to the oceanic lithosphere due to the interaction with a mantle plume (Seno & Yamanaka, 1996). The zone of hydrous minerals in the subducting slab, consisting of the metamorphosed oceanic crust and the serpentinized slab mantle above 150 km depth and the slab mantle with hydrous peridotite (serpentine or phase A) at greater depths (150–380 km), should be characterized with large to medium shear wave speed reduction compared to the average mantle (i.e., PREM or IASPEI91). While this low-wave speed zone is not revealed by continental-scale tomography due to resolution limitations, it has been observed previously with high-frequency waveform modeling beneath northeast Japan down to a depth of at least 300 km and maybe even deeper (Chen et al., 2007).

With the expected uncertainties in temperature estimation, the calculated P - T conditions of lower seismic zone earthquakes are scattered but approximately correlated with the conditions of a series of dehydration reactions at different depth ranges (Hacker et al., 2003; Omori et al., 2004; Figure 4), including antigorite dehydration I (antigorite = forsterite + enstatite + H₂O) and chlorite dehydration (chlorite + enstatite = forsterite + pyrope + H₂O) at depths of 100–200 km, antigorite dehydration II (antigorite = phase A + enstatite + H₂O) and phase A dehydration (phase A + enstatite + Mg-sursassite = pyrope + H₂O) at depths of 200–300 km, and phase A dehydration at depths 300–380 km. The correlations suggest that at depths of 100–200 km, in addition to antigorite dehydration, chlorite

dehydration likely also contributes to trigger earthquakes in the lower-plane seismic zones via fluid-related embrittlement (Figure 4). At depths of 150–200 km the seismogenic zone appears as a single seismic plane, with seismicity peak loci corresponding to temperatures of 400–900 °C (Figures 3c and 3d). We speculate that the disappearance of upper seismic zone at this depth range is due to two reasons: (1) hydrous minerals in the crust are completely dehydrated and eclogitized below 150 km (Abers et al., 2013) and (2) only the dehydration reactions at the lower dehydration foci of antigorite serpentine (possibly chlorite) contribute to trigger earthquakes because its upper dehydration loci are mostly located in the wedge mantle above the slab in this depth range (Yamasaki & Seno, 2003).

At greater depths of 200–300 km, the sudden widening of the seismogenic zone (Figure 3c) possibly indicates that a new hydrous phase, for example, phase A, starts to break down between temperatures of 600–700 °C and triggers earthquakes due to the fluid-related embrittlement at the higher P - T regime (Figure 4; Omori et al., 2004). The deep seismicity between 300 and 380 km may be associated with continued dehydration of phase A (Omori et al., 2004), because the 410-km discontinuity is only elevated up to 395-km depth due to the cold slab (Wang et al., 2017), and therefore, the phase transformational faulting of metastable olivine to wadsleyite (Kirby et al., 1991) is not a viable mechanism for these seismicity. The DSZ width decreases in the depth range of 300–380 km compared to the width at depths of 200–300 km, with seismicity concentrated in a slab-normal depth range of 15–30 km (Figure 3d), possibly suggesting a wedge-shaped Phase A layer tapering away with increasing P - T toward the slab cold core (Figure 4). This shape contradicts the idea that the Phase A dehydration boundaries possibly cut through isotherms (Hacker et al., 2003; Stalder & Ulmer, 2001) and is more consistent with the nearly isothermal phase boundary branch (~625–650 °C at depths of 200–380 km in Figures 4a and 4b) determined by Omori et al. (2004).

5. Conclusions

This study is unique in approximating the absolute slab-normal depths and determining the temperatures of the peak seismicity foci. We propose that the lower-plane seismogenesis at the depths between 100 and 380 km can be linked to a series of dehydration reactions of hydrated slab peridotites, including the breakdown of antigorite and chlorite (mainly clinocllore) at depths of 100–200 km, and the dehydration of phase A at depths of 200–380 km. Water released from these dehydration reactions contributes to the deep seismogenesis through fluid-related embrittlement.

Without a clear indication of the location of oceanic crust in tomographic models at greater depths, where the slab surface is located remains a challenging scientific problem to pursue. New tomographic techniques that can employ teleseismic high-frequency data such as P to S converted phases may provide a way to resolve finer slab internal interfaces. In order to more precisely determine spatial relationships between slab interfaces and deep intraslab earthquakes, we also need to accurately relocate deep earthquakes with refined 3-D slab models taken into account. The EARA2014 slab interface model is nevertheless an incremental improvement in understanding this relationship, which provides a baseline for higher resolution slab structure and earthquake source imaging studies. We anticipate such work will shed new light on the petrological and thermal state of not only the Pacific Plate beneath Japan but also other subducting slabs in similar tectonic settings.

References

- Abers, G. A. (2005). Seismic low-velocity layer at the top of subducting slabs: Observations, predictions, and systematics. *Physics of the Earth and Planetary Interiors*, 149(1-2), 7–29. <https://doi.org/10.1016/j.pepi.2004.10.002>
- Abers, G. A., Nakajima, J., van Keken, P. E., Kita, S., & Hacker, B. R. (2013). Thermal-petrological controls on the location of earthquakes within subducting plates. *Earth and Planetary Science Letters*, 369–370, 178–187. <https://doi.org/10.1016/j.epsl.2013.03.022>
- Bassin, C., Laske, G., & Masters, G. (2000). The current limits of resolution for surface wave tomography in North America. *Eos Transactions American Geophysical Union*, 81, F897.
- Bock, G., Schurr, B., & Asch, G. (2000). High-resolution image of the oceanic Moho. *Geophysical Research Letters*, 27(23), 3929–3932. <https://doi.org/10.1029/2000GL011881>
- Brudzinski, M. R., Thurber, C. H., Hacker, B. R., & Engdahl, E. R. (2007). Global prevalence of double Benioff zones. *Science*, 316(5830), 1472–1474. <https://doi.org/10.1126/science.1139204>
- Chen, M., Niu, F., Liu, Q., Tromp, J., & Zhen, X. (2015). Multiparameter adjoint tomography of the crust and upper mantle beneath East Asia: 1. gModel construction and comparisons. *Journal of Geophysical Research: Solid Earth*, 120, 1762–1786. <https://doi.org/10.1002/2014JB011638>

Acknowledgments

We thank the Editor (Jeroen Ritsma) and two anonymous reviewers for their constructive and insightful comments that helped improve the manuscript. We also thank one of the reviewers for providing the sentence on apparent slab gaps in tomographic models. The EHB catalog hypocenter location data were downloaded from the International Seismological Centre website (<http://www.isc.ac.uk/ehbulletin/search/catalogue/>). We thank the High Performance Computing Center (HPCC) at Michigan State University, the Extreme Science and Engineering Discovery Environment (XSEDE) supported by NSF grant ACI-1053575), and the National Laboratory for Advanced Scientific Visualization at UNAM (LAVIS) for providing the computational resources. Model EARA2014 used in this study is provided as supporting information dataset of this publication. We thank Susannah Dorfman, Yingcai Zheng, Zhongwen Zhan, Lijun Liu, Lingsen Meng, Saeko Kita, and Keishi Okazaki for their constructive discussion and suggestion. This research was supported by NSF grant 1802247, Romanian MNESR-STAR grant 513, and JST-JICA SATREPS grant 1554361.

- Chen, M., Tromp, J., Helmberger, D., & Kanamori, H. (2007). Waveform modeling of the slab beneath Japan. *Journal of Geophysical Research*, *112*, B02305. <https://doi.org/10.1029/2006JB004394>
- Contreras-Reyes, E., Grevemeyer, I., Watts, A. B., Flueh, E. R., Peirce, C., Moeller, S., & Papenberg, C. (2011). Deep seismic structure of the Tonga subduction zone: Implications for mantle hydration, tectonic erosion, and arc magmatism. *Journal of Geophysical Research*, *116*, B10103. <https://doi.org/10.1029/2011JB008434>
- DeMets, C., Gordon, R. G., & Argus, D. F. (2010). Geologically current plate motions. *Geophysical Journal International*, *181*(1), 1–80. <https://doi.org/10.1111/j.1365-246X.2009.04491.x>
- Dobson, D. P., Meredith, P. G., & Boon, S. A. (2002). Simulation of subduction zone seismicity by dehydration of serpentine. *Science*, *298*, 1407–1410. <https://doi.org/10.1126/science.1075390>
- Ekström, G., Dziewoński, A. M., Maternovskaya, N. N., & Nettles, M. (2005). Global seismicity of 2003: Centroid–moment–tensor solutions for 1087 earthquakes. *Physics of the Earth and Planetary Interiors*, *148*(2–4), 327–351. <https://doi.org/10.1016/j.pepi.2004.09.006>
- Engdahl, E., Dewey, J., & Fujita, K. (1982). Earthquake location in island arcs. *Physics of the Earth and Planetary Interiors*, *30*(2–3), 145–156. [https://doi.org/10.1016/0031-9201\(82\)90099-1](https://doi.org/10.1016/0031-9201(82)90099-1)
- Engdahl, E. R., & Scholz, C. H. (1977). A double Benioff Zone beneath the central Aleutians: An unbending of the lithosphere. *Geophysical Research Letters*, *4*(10), 473–476. <https://doi.org/10.1029/GL004i010p00473>
- Engdahl, E. R., van der Hilst, R., & Buland, R. (1998). Global teleseismic earthquake relocation with improved travel times and procedures for depth determination. *Bulletin of the Seismological Society of America*, *88*(3), 722–743. <https://doi.org/10.1130/0-8137-2349-3.461>
- Faccenda, M., Gerya, T. V., Mancktelow, N. S., & Moresi, L. (2012). Fluid flow during slab unbending and dehydration: Implications for intermediate-depth seismicity, slab weakening and deep water recycling. *Geochemistry, Geophysics, Geosystems*, *13*, Q01010. <https://doi.org/10.1029/2011GC003860>
- Fichtner, A., & Trampert, J. (2011). Hessian kernels of seismic data functionals based upon adjoint techniques. *Geophysical Journal International*, *185*(2), 775–798. <https://doi.org/10.1111/j.1365-246X.2011.04966.x>
- Fujie, G., Kodaira, S., Kaiho, Y., Yamamoto, Y., Takahashi, T., Miura, S., & Yamada, T. (2018). Controlling factor of incoming plate hydration at the north-western Pacific margin. *Nature Communications*, *9*(1), 3844. <https://doi.org/10.1038/s41467-018-06320-z>
- Fukao, Y., & Obayashi, M. (2013). Subducted slabs stagnant above, penetrating through, and trapped below the 660 km discontinuity. *Journal of Geophysical Research: Solid Earth*, *118*, 5920–5938. <https://doi.org/10.1002/2013JB010466>
- Green, H. W., & Houston, H. (1995). The mechanics of deep earthquakes. *Annual Review of Earth and Planetary Sciences*, *23*(1), 169–213. <https://doi.org/doi:10.1146/annurev.ea.23.050195.001125>
- Gudmundsson, Ö., & Sambridge, M. (1998). A regionalized upper mantle (RUM) seismic model. *Journal of Geophysical Research*, *103*(B4), 7121–7136. <https://doi.org/10.1029/97JB02488>
- Hacker, B. R., Peacock, S. M., Abers, G. A., & Holloway, S. D. (2003). Subduction factory 2. Are intermediate-depth earthquakes in subducting slabs linked to metamorphic dehydration reactions? *Journal of Geophysical Research*, *108*(B1), 2030. <https://doi.org/10.1029/2001JB001129>
- Hasegawa, A., Horiuchi, S., & Unimo, N. (1994). Seismic structure of the northeastern Japan convergent margin: A synthesis. *Journal of Geophysical Research*, *99*(B11), 22,295–22,311. <https://doi.org/10.1029/93JB02797>
- Hasegawa, A., & Nakajima, J. (2017). Seismic imaging of slab metamorphism and genesis of intermediate-depth intraslab earthquakes. *Progress in Earth and Planetary Science*, *4*(1). <https://doi.org/10.1186/s40645-017-0126-9>
- Hasegawa, A., Umio, N., & Takagi, A. (1978). Double-planned deep seismic zone and upper-mantle structure in the northeastern Japan arc. *Geophysical Journal of the Royal Astronomical Society*, *54*(2), 281–296. <https://doi.org/10.1111/j.1365-246X.1978.tb04260.x>
- Hayes, G. P., Wald, D. J., & Johnson, R. L. (2012). Slab1.0: A three-dimensional model of global subduction zone geometries. *Journal of Geophysical Research*, *117*, B01302. <https://doi.org/10.1029/2011JB008524>
- Hjörleifsdóttir, V., & Ekström, G. (2010). Effects of three-dimensional Earth structure on CMT earthquake parameters. *Physics of the Earth and Planetary Interiors*, *179*(3–4), 178–190. <https://doi.org/10.1016/j.pepi.2009.11.003>
- Hobbs, B. E., & Ord, A. (1988). Plastic instabilities: Implications for the origin of intermediate and deep focus earthquakes. *Journal of Geophysical Research*, *93*(B9), 10,521–10,540. <https://doi.org/10.1029/JB093iB09p10521>
- Igarashi, T., Matsuzawa, T., Umio, N., & Hasegawa, A. (2001). Spatial distribution of focal mechanisms for interplate and intraplate earthquakes associated with the subducting Pacific plate beneath the northeastern Japan arc: A triple-planned deep seismic zone. *Journal of Geophysical Research*, *106*(B2), 2177–2191. <https://doi.org/10.1029/2000JB900386>
- John, T., Medvedev, S., Rüpke, L. H., Andersen, T. B., Podladchikov, Y. Y., & Austrheim, H. (2009). Generation of intermediate-depth earthquakes by self-localizing thermal runaway. *Nature Geoscience*, *2*(2), 137–140. <https://doi.org/10.1038/ngeo419>
- Jung, H., Green, H. W., & Dobrzhinetskaya, L. F. (2004). Intermediate-depth earthquake faulting by dehydration embrittlement with negative volume change. *Nature*, *428*(6982), 545–549. <https://doi.org/10.1038/nature02412>
- Kao, H., & Liu, L.-G. (1995). A hypothesis for the seismogenesis of a double seismic zone. *Geophysical Journal International*, *123*, 71–84. <https://doi.org/10.1111/j.1365-246X.1995.tb06662.x>
- Kao, H., & Ruey-Juin, R. (1999). Detailed structures of the subducted Philippine Sea plate beneath northeast Taiwan: A new type of double seismic zone. *Journal of Geophysical Research*, *104*(B1), 1015–1033. <https://doi.org/10.1029/1998JB900010>
- Karato, S., Riedel, M. R., & Yuen, D. A. (2001). Rheological structure and deformation of subducted slabs in the mantle transition zone: Implications for mantle circulation and deep earthquakes. *Physics of the Earth and Planetary Interiors*, *127*, 83–108. [https://doi.org/10.1016/S0031-9201\(01\)00223-0](https://doi.org/10.1016/S0031-9201(01)00223-0)
- Kawakatsu, H. (1985). Double seismic zone in Tonga. *Nature*, *316*(6023), 53–55. <https://doi.org/10.1038/316053a0>
- Kawakatsu, H., & Yoshioka, S. (2011). Metastable olivine wedge and deep dry cold slab beneath southwest Japan. *Earth and Planetary Science Letters*, *303*(1–2), 1–10. <https://doi.org/10.1016/j.epsl.2011.01.008>
- Kirby, S., Engdahl, E. R., & Denlinger, R. (1996). Intermediate-depth intraslab earthquakes and arc volcanism as physical expressions of crustal and uppermost mantle metamorphism in subducting slabs. In G. E. Bebout, D. W. Scholl, S. H. Kirby, & J. P. Platt (Eds.), *Subduction: Top to bottom, Geophysical Monograph Series* (Vol. 96, pp. 195–213). Washington, DC: American Geophysical Union. <https://doi.org/10.1029/GM096p0195>
- Kirby, S. H., Durham, W. B., & Stern, L. A. (1991). Mantle phase changes and deep-earthquake faulting in subducting lithosphere. *Science*, *252*(5003), 216–225. <https://doi.org/10.1126/science.252.5003.216>
- Kisslinger, C. (1993). Seismicity in subduction zones from local and regional network observations. *Pure and Applied Geophysics*, *140*(2), 257–285. <https://doi.org/10.1007/BF00879407>
- Kita, S., & Ferrand, T. P. (2018). Physical mechanisms of oceanic mantle earthquakes: Comparison of natural and experimental events. *Scientific Reports*, *8*(1), 17049. <https://doi.org/10.1038/s41598-018-35290-x>

- Kita, S., Okada, T., Hasegawa, A., Nakajima, J., & Matsuzawa, T. (2010). Existence of interplane earthquakes and neutral stress boundary between the upper and lower planes of the double seismic zone beneath Tohoku and Hokkaido, northeastern Japan. *Tectonophysics*, 496(1-4), 68–82. <https://doi.org/10.1016/j.tecto.2010.10.010>
- Kita, S., Okada, T., Nakajima, J., Matsuzawa, T., & Hasegawa, A. (2006). Existence of a seismic belt in the upper plane of the double seismic zone extending in the along-arc direction at depths of 70–100 km beneath NE Japan. *Geophysical Research Letters*, 33, L24310. <https://doi.org/10.1029/2006GL028239>
- Komatitsch, D., & Tromp, J. (2002a). Spectral-element simulations of global seismic wave propagation—I. Validation. *Geophysical Journal International*, 149(2), 390–412. <https://doi.org/10.1046/j.1365-246X.2002.01653.x>
- Komatitsch, D., & Tromp, J. (2002b). Spectral-element simulations of global seismic wave propagation—II. Three-dimensional models, oceans, rotation and self-gravitation. *Geophysical Journal International*, 150(1), 303–318. <https://doi.org/10.1046/j.1365-246X.2002.01716.x>
- Kumar, P., & Kawakatsu, H. (2011). Imaging the seismic lithosphere-asthenosphere boundary of the oceanic plate. *Geochemistry, Geophysics, Geosystems*, 12, Q01006. <https://doi.org/10.1029/2010GC003358>
- Kustowski, B., Ekström, G., & Dziewoński, A. M. (2008). Anisotropic shear-wave velocity structure of the Earth's mantle: A global model. *Journal of Geophysical Research*, 113, B06306. <https://doi.org/10.1029/2007JB005169>
- Liu, Q., Polet, J., Komatitsch, D., & Tromp, J. (2004). Spectral-element moment tensor inversions for earthquakes in Southern California. *Bulletin of the Seismological Society of America*, 94(5), 1748–1761. <https://doi.org/10.1785/012004038>
- Liu, Q., & Tromp, J. (2006). Finite-frequency kernels based on adjoint methods. *Bulletin of the Seismological Society of America*, 96(6), 2383–2397. <https://doi.org/10.1785/0120060041>
- Liu, Q., & Tromp, J. (2008). Finite-frequency sensitivity kernels for global seismic wave propagation based upon adjoint methods. *Geophysical Journal International*, 174(1), 265–286. <https://doi.org/10.1111/j.1365-246X.2008.03798.x>
- Liu, X., & Zhao, D. (2016). P and S wave tomography of Japan subduction zone from joint inversions of local and teleseismic travel times and surface-wave data. *Physics of the Earth and Planetary Interiors*, 252, 1–22. <https://doi.org/10.1016/j.pepi.2016.01.002>
- Maggi, A., Tape, C., Chen, M., Chao, D., & Tromp, J. (2009). An automated time-window selection algorithm for seismic tomography. *Geophysical Journal International*, 178(1), 257–281. <https://doi.org/10.1111/j.1365-246X.2009.04099.x>
- Manea, V. C., Manea, M., Kostoglodov, V., Currie, C. A., & Sewell, G. (2004). Thermal structure, coupling and metamorphism in the Mexican subduction zone beneath Guerrero. *Geophysical Journal International*, 158(2), 775–784. <https://doi.org/10.1111/j.1365-246X.2004.02325.x>
- McGuire, J. J., & Wiens, D. A. (1995). A double seismic zone in New Britain and the morphology of the Solomon Plate at intermediate depths. *Geophysical Research Letters*, 22(15), 1965–1968. <https://doi.org/10.1029/95GL01806>
- Meng, L., Ampuero, J.-P., & Bürgmann, R. (2014). The 2013 Okhotsk deep-focus earthquake: Rupture beyond the metastable olivine wedge and thermally controlled rise time near the edge of a slab. *Geophysical Research Letters*, 41, 3779–3785. <https://doi.org/10.1002/2014GL059968>
- Müller, R. D., Sdrorlias, M., Gaina, C., & Roest, W. R. (2008). Age, spreading rates, and spreading asymmetry of the world's ocean crust. *Geochemistry, Geophysics, Geosystems*, 9, Q04006. <https://doi.org/10.1029/2007GC001743>
- Nakajima, J., Tsuji, Y., & Hasegawa, A. (2009). Seismic evidence for thermally-controlled dehydration reaction in subducting oceanic crust. *Geophysical Research Letters*, 36, L03303. <https://doi.org/10.1029/2008GL036865>
- National Geophysical Data Center. (2006). 2-minute gridded global relief data (ETOPO2v2).
- Obayashi, M., Yoshimitsu, J., Nolet, G., Fukao, Y., Shiobara, H., Sugioka, H., Miyamachi, H., et al. (2013). Finite frequency whole mantle P wave tomography: Improvement of subducted slab images. *Geophysical Research Letters*, 40, 5652–5657. <https://doi.org/10.1002/2013GL057401>
- Ohuchi, T., Lei, X., Ohfuji, H., Higo, Y., Tange, Y., Sakai, T., et al. (2017). Intermediate-depth earthquakes linked to localized heating in dunite and harzburgite. *Nature Geoscience*, 10(10), 771–776. <https://doi.org/10.1038/ngeo3011>
- Okazaki, K., & Hirth, G. (2016). Dehydration of lawsonite could directly trigger earthquakes in subducting oceanic crust. *Nature*, 530(7588), 81–84. <https://doi.org/10.1038/nature16501>
- Omori, S., Komabayashi, T., & Maruyama, S. (2004). Dehydration and earthquakes in the subducting slab: Empirical link in intermediate and deep seismic zones. *Physics of the Earth and Planetary Interiors*, 146(1-2), 297–311. <https://doi.org/10.1016/j.pepi.2003.08.014>
- Peacock, S. M. (2001). Are the lower planes of double seismic zones caused by serpentine dehydration in subducting oceanic mantle? *Geology*, 29(4), 299–302. [https://doi.org/10.1130/0091-7613\(2001\)029<0299:ATLPOD>2.0.CO;2](https://doi.org/10.1130/0091-7613(2001)029<0299:ATLPOD>2.0.CO;2)
- Ranero, C. R., Phipps Morgan, J., McIntosh, K., & Relchert, C. (2003). Bending-related faulting and mantle serpentinization at the Middle America trench. *Nature*, 425(6956), 367–373. <https://doi.org/10.1038/nature01961>
- Schaeffer, A. J., & Lebedev, S. (2013). Global shear speed structure of the upper mantle and transition zone. *Geophysical Journal International* <https://doi.org/10.1093/gji/ggt095>, 194(1), 417–449.
- Seno, T., & Yamanaka, Y. (1996). Double seismic zones, compressional deep trench-outer rise events, and superplumes. In *Subduction: Top to bottom*, *Geophysical Monograph* (Vol. 96, pp. 347–355). Washington, DC: American Geophysical Union.
- Shiina, T., Nakajima, J., & Matsuzawa, T. (2013). Seismic evidence for high pore pressures in the oceanic crust: Implications for fluid-related embrittlement. *Geophysical Research Letters*, 40, 2006–2010. <https://doi.org/10.1002/grl.50468>
- Shillington, D. J., Becel, A., Nedimovic, M. R., Kuehn, H., Webb, S. C., Abers, G. A., et al. (2015). Link between plate fabric, hydration and subduction zone seismicity in Alaska. *Nature Geoscience*, 8(12), 961–964. <https://doi.org/10.1038/ngeo2586>
- Smith, G. P., & Ekström, G. (1997). Interpretation of earthquake epicenter and CMT centroid locations, in terms of rupture length and direction. *Physics of the Earth and Planetary Interiors*, 102(1-2), 123–132. [https://doi.org/10.1016/S0031-9201\(96\)03246-3](https://doi.org/10.1016/S0031-9201(96)03246-3)
- Stalder, R., & Ulmer, P. (2001). Phase relations of a serpentine composition between 5 and 14 GPa: Significance of clinohumite and phase E as water carriers into the transition zone. *Contributions to Mineralogy and Petrology*, 140(6), 670–679. <https://doi.org/10.1007/s004100000208>
- Stein, C. A., & Stein, S. (1992). A model for the global variation in oceanic depth and heat flow with lithospheric age. *Nature*, 359(6391), 123–129. <https://doi.org/10.1038/359123a0>
- Syracuse, E. M., & Abers, G. A. (2006). Global compilation of variations in slab depth beneath arc volcanoes and implications. *Geochemistry, Geophysics, Geosystems*, 7, Q05017. <https://doi.org/10.1029/2005GC001045>
- Syracuse, E. M., van Keken, P. E., Abers, G. A., Suetsugu, D., Bina, C., Inoue, T., et al. (2010). The global range of subduction zone thermal models. *Physics of the Earth and Planetary Interiors*, 183(1-2), 73–90. <https://doi.org/10.1016/j.pepi.2010.02.004>
- Tape, C., Liu, Q., Maggi, A., & Tromp, J. (2009). Adjoint tomography of the Southern California crust. *Science*, 325, 988–992. <https://doi.org/10.1126/science.1175298>

- Tape, C., Liu, Q., Maggi, A., & Tromp, J. (2010). Seismic tomography of the Southern California crust based on spectral-element and adjoint methods. *Geophysical Journal International*, *180*(1), 433–462. <https://doi.org/10.1111/j.1365-246X.2009.04429.x>
- Tromp, J., Tape, C., & Liu, Q. (2005). Seismic tomography, adjoint methods, time reversal and banana-doughnut kernels. *Geophysical Journal International*, *160*(1), 195–216. <https://doi.org/10.1111/j.1365-246X.2004.02453.x>
- Tsuji, Y., Nakajima, J., & Hasegawa, A. (2008). Tomographic evidence for hydrated oceanic crust of the Pacific slab beneath northeastern Japan: Implications for water transportation in subduction zones. *Geophysical Research Letters*, *35*, L14308. <https://doi.org/10.1029/2008GL034461>
- Utsu, T. (1975). Regional variation of travel-time residuals of P waves from nearby deep earthquakes in Japan and vicinity. *Journal of Physics of the Earth*, *23*(4), 367–380. <https://doi.org/10.4294/jpe1952.23.367>
- van Avendonk, H. J. A., Holbrook, W. S., Lizaralde, D., & Denyer, P. (2011). Structure and serpentinization of the subducting Cocos plate offshore Nicaragua and Costa Rica. *Geochemistry, Geophysics, Geosystems*, *12*, Q06009. <https://doi.org/10.1029/2011GC003592>
- Van Keken, P. E., Kita, S., & Nakajima, J. (2012). Thermal structure and intermediate-depth seismicity in the Tohoku-Hokkaido subduction zones. *Solid Earth*, *3*(2), 355–364. <https://doi.org/10.5194/se-3-355-2012>
- Wang, X., Li, J., & Chen, Q. F. (2017). Topography of the 410 km and 660 km discontinuities beneath the Japan Sea and adjacent regions by analysis of multiple-ScS waves. *Journal of Geophysical Research: Solid Earth*, *122*, 1264–1283. <https://doi.org/10.1002/2016JB013357>
- Wei, S. S., Wiens, D. A., van Keken, P. E., & Cai, C. (2017). Slab temperature controls on the Tonga double seismic zone and slab mantle dehydration. *Science Advances*, *3*(January), e1601755. <https://doi.org/10.1126/sciadv.1601755>
- Wei, W., Xu, J., Zhao, D., & Shi, Y. (2012). East Asia mantle tomography: New insight into plate subduction and intraplate volcanism. *Journal of Asian Earth Sciences*, *60*, 88–103. <https://doi.org/10.1016/j.jseas.2012.08.001>
- Yamasaki, T., & Seno, T. (2003). Double seismic zone and dehydration embrittlement of the subducting slab. *Journal of Geophysical Research*, *108*(B4), 2212. <https://doi.org/10.1029/2002JB001918>
- Zhan, Z., Kanamori, H., Tsai, V. C., Helmberger, D. V., & Wei, S. (2014). Rupture complexity of the 1994 Bolivia and 2013 Sea of Okhotsk deep earthquakes. *Earth and Planetary Science Letters*, *385*, 89–96. <https://doi.org/10.1016/j.epsl.2013.10.028>
- Zhang, H., Thurber, C. H., Shelly, D., Ide, S., Beroza, G. C., & Hasegawa, A. (2004). High-resolution subducting-slab structure beneath northern Honshu, Japan, revealed by double-difference tomography. *Geology*, *32*(4), 361. <https://doi.org/10.1130/G20261.2>
- Zheng, X., Ouyang, B., Zhang, D., Yao, Z., Liang, J., & Zheng, J. (2009). Technical system construction of Data Backup Centre for China Seismograph Network and the data support to researches on the Wenchuan earthquake. *Chinese Journal of Geophysics* (in Chinese), *52*(5), 1412–1417. <https://doi.org/10.3969/j.issn.0001-5733.2009.05.031>
- Zhu, H., Bozdağ, E., Peter, D., & Tromp, J. (2012). Structure of the European upper mantle revealed by adjoint tomography. *Nature Geoscience*, *5*(7), 493–498. <https://doi.org/10.1038/ngeo1501>